





## Article

# Detection of Volatile Alcohol Vapors Using PMMA-Coated Micromechanical Sensors: Experimental and Quantum Chemical DFT Analysis

Reem A. Alsaigh <sup>1,†</sup>, Shofiur Rahman <sup>2,†</sup> , Fatimah S. Alfaihi <sup>1</sup>, Mahmoud A. Al-Gawati <sup>1,2</sup>, Raghad Shallaa <sup>1</sup>, Fatimah Alzaid <sup>1</sup>, Amal F. Alanazi <sup>2,3</sup>, Hamad Albrithen <sup>1,2</sup>, Khalid E. Alzahrani <sup>1,2</sup> , Abdulaziz K. Assaifan <sup>2</sup>, Abdullah N. Alodhayb <sup>1,2</sup>  and Paris E. Georghiou <sup>4,\*</sup> 

<sup>1</sup> Department of Physics and Astronomy, College of Science, King Saud University, Riyadh 11451, Saudi Arabia

<sup>2</sup> Biological and Environmental Sensing Research Unit, King Abdullah Institute for Nanotechnology, King Saud University, Riyadh 11451, Saudi Arabia

<sup>3</sup> Energy, Water, and Environment Lab, Faculty of Humanities and Sciences, Prince Sultan University, Riyadh 11586, Saudi Arabia

<sup>4</sup> Department of Chemistry, Memorial University of Newfoundland, St. John's, NL A1B 3X7, Canada

\* Correspondence: parisg@mun.ca

† These authors contributed equally to this work.



**Citation:** Alsaigh, R.A.; Rahman, S.; Alfaihi, F.S.; Al-Gawati, M.A.; Shallaa, R.; Alzaid, F.; Alanazi, A.F.; Albrithen, H.; Alzahrani, K.E.; Assaifan, A.K.; et al. Detection of Volatile Alcohol Vapors Using PMMA-Coated Micromechanical Sensors: Experimental and Quantum Chemical DFT Analysis. *Chemosensors* **2022**, *10*, 452. <https://doi.org/10.3390/chemosensors10110452>

Academic Editor: Masanori Ando

Received: 22 August 2022

Accepted: 15 October 2022

Published: 1 November 2022

**Publisher's Note:** MDPI stays neutral with regard to jurisdictional claims in published maps and institutional affiliations.



**Copyright:** © 2022 by the authors. Licensee MDPI, Basel, Switzerland. This article is an open access article distributed under the terms and conditions of the Creative Commons Attribution (CC BY) license (<https://creativecommons.org/licenses/by/4.0/>).

**Abstract:** Micromechanical sensors, in which the sensor response is created as a result of molecular interactions on the sensors' surfaces, have been employed as a powerful technique for rapid and sensitive detection of low concentrations of chemical and biological materials. In the study reported herein, poly(methyl methacrylate) (PMMA)-coated microcantilever (MCL) sensors were used to detect the vapors of volatile alcohols (methanol, ethanol, and isopropanol) at three different concentrations. A vapor generator was used to generate and flow the alcohol vapor onto the PMMA coated MCL surface in a closed system chamber. The vapor adsorption onto the MCL surface results in a rapid and measurable deflection of the MCL. No significant deflections of the uncoated MCL occurred when the different vapors were passed through into the microcantilever chamber. Linear concentration-deflection responses were observed, with the highest sensitivity shown with methanol, followed by ethanol and then isopropanol. Density functional theory (DFT) quantum chemical calculations were conducted to estimate the electronic interaction energies ( $\Delta IE$ ) between the alcohol molecules and MMA and two different model tetrameric segments of PMMA. The computed  $\Delta IEs$  were in the same order as the experimentally observed order: methanol > ethanol > isopropanol.

**Keywords:** microcantilever sensor; poly(methyl methacrylate) (PMMA); volatile alcohols; vapor generator; density functional theory (DFT)

## 1. Introduction

Volatile organic compounds (VOCs) are found ubiquitously in our immediate environments [1] and are mainly linked with emissions from transportation and industrial processes. VOCs result from the use of organic solvents and many different industrial organic chemicals, which are widely used [2] as ingredients for pharmaceuticals, pesticides, plastics, fuels [3], solvents, explosives, surface coatings, adhesives, disinfectants, and fire retardants. All of these substances have the potential to emit and disperse volatile organic molecules into the surrounding environments during their use and storage. Due to their potential global and human health effects [4], even at the relatively low concentrations of VOCs released into the atmosphere, their detection and monitoring are very important. This also includes detecting and monitoring VOCs in indoor air environments where humans spend many hours daily. The sources of VOCs encountered in domestic or office and non-industrial workplace indoor air include solvents from cleaning products, personal

cosmetic and hair product use materials, formaldehyde emissions from synthetic fibers and/or furniture and flooring laminates, printer and photocopier use, paints, cooking, and tobacco or other smoking product use [5–7]. Analyses of VOCs obtained from breath samples have been associated with certain diseases and used as biomarkers for disease diagnoses [8,9].

Some alcohols such as methanol, ethanol, ethylene glycol, diethylene glycol, isopropanol, etc., [10] are also commonly encountered as VOCs in a variety of domestic, office, and non-industrial and industrial workplace indoor air environments. In principle, toxic exposure to these alcohols can occur through skin absorption, inhalation, or ingestion, and the routes of exposure depend on the type of alcohol(s) involved [11]. Although the most common route of exposure for methanol, ethanol, and isopropanol, which are the subject alcohols in this study, is direct ingestion, exposure by inhalation to these compounds as VOC components can also occur in indoor air environments. The toxicity of these alcohols arises due to their metabolic breakdown products, including their corresponding aldehydes and, in the case of isopropanol, to acetone [10,11].

The detection of VOCs has been conducted with many different analytical methods which have employed, for example, photoionization [12], surface acoustic wave sensors [13,14], field-effect transistors [15], calorimetry [16], gas chromatography [17], and infrared spectroscopy [18]. In recent years, microcantilevers (MCLs) which can be operated in static or dynamic modes, have been used as sensitive transducers in a variety of applications. These include the detection of VOCs [19–23] and other trace volatile organic amines [24]. The adsorption of analyte vapors on exposed MCL surfaces, which have been coated with various polymers which can be easily applied using either spray, drop, or spin coating processes, have been shown to be enhanced. Examples of such MCL polymer coatings which have been reported include gelatin [19]; polydimethylsiloxane [20]; polyethylene oxide, polyethylenevinylacetate (PEVA), polyvinyl alcohol (PVA) [22]; polymethylmethacrylate (PMMA) [25–27], and polyaniline [28]. All of these have shown good reproducibility and are linearly proportional to VOC concentrations. Since there are significant differences in the hydrophilicity and hydrophobicity of the polymers and their suitability for the diffusion of polar and nonpolar analyte molecules, the type of polymer selected for the detection of specific VOCs is critical. The MCL surface for gas molecular sensing must have a functional group able to detect the specified chemical based on adsorption/desorption principles.

In this study, we investigated the use of polymethyl methacrylate (PMMA) as a potential low-concentration VOC sensing layer. We report herein on the study we conducted using the static mode detection of different concentrations of three representative VOCs, namely methanol, ethanol, and isopropanol, using PMMA-coated MCL sensors. The alcohol samples analyzed were vaporized using a customized steady-state stream vapor = generating system linked to the microcantilever sensor chamber. To provide further insight into our experimental findings, we conducted Density Functional Theory (DFT) computations using model systems based upon a mechanism for our hypothesized mode of adsorption of the alcohol vapors onto the PMMA-coated MCLs.

## 2. Materials and Methods

### 2.1. Chemicals and Materials

Methanol, ethanol, isopropanol, hydrogen peroxide (H<sub>2</sub>O<sub>2</sub>), sulfuric acid, and polymethyl methacrylate (PMMA) were purchased from Sigma Aldrich. All solvents and reagents were of analytical or reagent grade and were used as received. The silicon MCL arrays used in this study were purchased from Micromotive (Germany). Each array consists of eight individual 500 ± 5 μm × 90 ± 2 μm × 1 ± 0.3 μm MCLs.

### 2.2. Experimental Setup and Instrumentation

The experimental setup consisted of a customized vapor generator system and a Picomeasure PM3 (both from Fourien Inc, Edmonton, AB, Canada), and is depicted in the

schematic shown (Figure 1). The vapor generator system was used to deliver the nitrogen carrier gas and to generate the volatile liquid analytes. In this system, a microcantilever was mounted on a closed sensing chamber, and a laser beam was allowed to focus on the free end of the MCL. The reflective laser beam was then focused on a position sensitive detection (PSD), which translates the mechanical deflection signal into an electrical one. A detailed description of the PM3 is discussed elsewhere [29]. The Picomeasure PM3 device [30] was used to measure the microcantilever deflection. The nitrogen carrier gas was channeled using a mass flow controller to deliver a flow rate of 100 mL/min. The flow rate, temperature, and other parameters are controlled directly via the Picomeasure PM3 instrument. The nitrogen gas was transferred from the mass flow controller to a vapor generating glass chamber containing the target alcohol analyte. The temperature of the MCL chamber was 23 °C and was also controlled via the Picomeasure PM3 instrument.

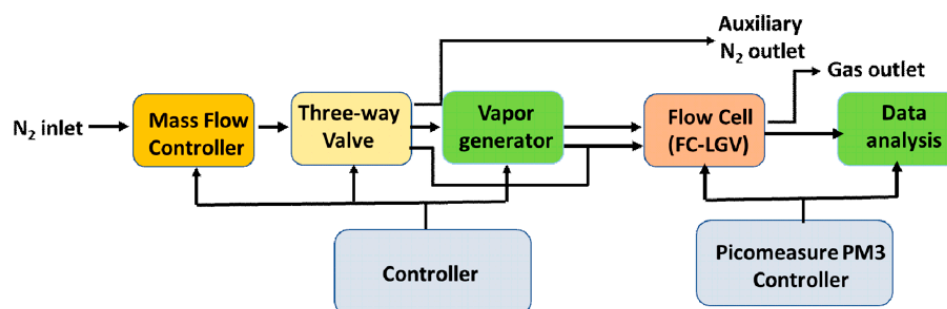


**Figure 1.** Schematical illustration of the measurement system (Picomeasure PM3).

To remove any organic contaminants before immobilizing PMMA onto the MCLs, the MCLs were pre-treated for 5 min by rinsing with piranha solution (3 parts of concentrated sulfuric acid and 1 part 30 wt. % hydrogen peroxide solution), followed by rinsing with distilled–deionized water and then ethanol. The MCLs were then dried for 10 min at 250 °C and then cooled to room temperature in a desiccator. A PMMA solution was prepared by mixing PMMA (0.50 g) with chloroform (100 g) and stirred using a magnetic stirrer for 1 h to form a homogenous solution. The cleaned MCL arrays were immersed in the PMMA solution for 5 min and then placed in a desiccator, where they were maintained at room temperature for 24 h before being used. The average thickness of the PMMA layer on the MCLs surface was  $55 \pm 5$  nm, as measured with a Bruker Dektak XT surface profiler.

Steady-state vapor streams of the alcohols were generated by passing the nitrogen carrier gas over a reservoir of the liquid alcohol in the glass vapor-generating chamber. The chamber volume was 25.0 mL and was heated with an external water bath set at three different temperatures (23, 30, and 35 °C) to generate the three different concentrations of the tested alcohol vapors. The volume of the analyte alcohol (methanol, ethanol, or isopropanol) in the vapor-generating chamber was fixed at 6.0 mL. For each determination, a fixed volume of the dry nitrogen gas (controlled with the flow rate of 100 mL/min) was injected into the vapor generator to vaporize the respective alcohol analyte, which was then channeled by the carrier gas into the microcantilever chamber. The PM3 Picomeasure instrument [30] containing the PMMA-coated MCL measures the deflection using a laser beam passing through the optical windows at the top of the flow cell and was focused onto a single MCL in the array.

Since a constant stream of the carrier gas was passed over the alcohol in the reservoir, a steady state of the vapor phase of the alcohol was maintained and was dependent only on the temperatures of the liquid. It was therefore estimated that the number of molecules of the vapor reaching the MCLs was equal to the corresponding value, which was calculated using the ideal gas law, where the number of moles of the vapor  $n = (PV)/(RT)$  and where  $P$  = vapor pressure (kPa) of the alcohol at  $T$  (K) and  $V$  = volume (25.0 mL  $\pm$  5%) of the space in which the vapor + carrier gas is generated, and  $R = 8.314$  L kPa/mol K.

### 2.3. Density Functional Theory (DFT) Calculations

All gas phase computational calculations were conducted with *Gaussian 16, Revision C.01* [31] at the B3LYP/6-311++G(d,p) level of theory. To understand the effect of the noncovalent interaction energies of the complexes, we also computed the interaction energies using the basis set superposition error (BSSE) [32] correction with a counterpoise of the complexes that were optimized in the gas phase at the B3LYP/6-311++G(d,p) level of theory. A vibrational analysis was conducted for each optimized molecule to ensure that they were in a vibrational energy minimum and had no imaginary frequencies. Using Equations (1) or (2), gas phase interaction energy ( $\Delta IE$ ) values were calculated from the electronic energies [31] of the components for the hypothetical modeled complexes formed: (i) with a monomeric MMA with a single alcohol molecule; and (ii) with the respective modeled tetrameric segments (“s-TMMA” or “a-TMMA”) of PMMA, as shown in Figure 2 where  $n = 4$ ) and as discussed further in Section 3.2 below.

$$\Delta IE = E_{[\text{MMA}] \supset [\text{analyte}]} - (E_{[\text{MMA}]} + E_{[\text{analyte}]}) \quad (1)$$

$$\Delta IE = E_{[\text{TMMA}] \supset [\text{analyte}]} - (E_{[\text{TMMA}]} + E_{[\text{analyte}]}) \quad (2)$$

where,  $E_{[\text{MMA}] \supset [\text{analyte}]}$  = optimized energy of the MMA complex with analyte alcohol;  $E_{[\text{MMA}]}$  = optimized electronic energy of the free monomer MMA;  $E_{[\text{PMMA}] \supset [\text{analyte}]}$  = optimized electronic energy of the tetrameric complex(es) with 1–4 molecules of the analyte;  $E_{[\text{TMMA}]}$  = optimized electronic energy of the free TMMA or TMMA segment(s); and  $E_{[\text{analyte}]}$  = optimized electronic energy of the individual analytes (methanol, ethanol or isopropanol).

Additional quantum chemical parameters were also calculated from the optimized most stable geometries of the species examined: (a)  $E_{\text{HOMO}}$  and  $E_{\text{LUMO}}$  frontier molecular orbitals (FMO) [33] generated using *GaussView 6.0.16* software and their energies. From Koopmans’ theorem [34,35], the  $E_{\text{HOMO}}$  of a species gives a measure of its ionization potential (IP) and is a characteristic of its nucleophilicity. The corresponding  $E_{\text{LUMO}}$  is related to the negative of the electron affinity (EA) and is a measure of the species’ susceptibility towards reacting with electrophiles, i.e.,  $E_{\text{HOMO}} = -IP$ ; and  $E_{\text{LUMO}} = -EA$ .

The energy gap ( $\Delta E_{\text{HOMO-LUMO}}$ ) is related to the polarizability of the species, and the large HOMO-LUMO gap indicates high stability and low chemical reactivity. Other quantum chemical properties which give a measure of chemical reactivity were also determined from the HOMO-LUMO energy values. These included global hardness ( $\eta$ ), global softness ( $S$ ), electronegativity ( $\chi$ ), chemical potential ( $\mu$ ), and electrophilicity index ( $\omega$ ), which can be calculated using the respective Equations (3)–(7):

$$\eta = \left[ \frac{E_{\text{LUMO}} - E_{\text{HOMO}}}{2} \right] = \left[ \frac{IP - EA}{2} \right] \quad (3)$$

$$S = \left[ \frac{2}{E_{\text{LUMO}} - E_{\text{HOMO}}} \right] = \left[ \frac{2}{IP - EA} \right] = \frac{1}{\eta} \quad (4)$$

$$\chi = \left[ \frac{E_{\text{LUMO}} + E_{\text{HOMO}}}{2} \right] = \left[ \frac{IP + EA}{2} \right] \quad (5)$$

$$\mu = \left[ \frac{E_{\text{HOMO}} + E_{\text{LUMO}}}{2} \right] = - \left[ \frac{IP + EA}{2} \right] \quad (6)$$

$$\omega = \frac{\chi^2}{2\eta} = \left[ \frac{\left( \frac{E_{\text{HOMO}} + E_{\text{LUMO}}}{2} \right)^2}{(E_{\text{LUMO}} - E_{\text{HOMO}})} \right] = \left[ \frac{\left( \frac{IP + EA}{2} \right)^2}{IP - EA} \right] \quad (7)$$

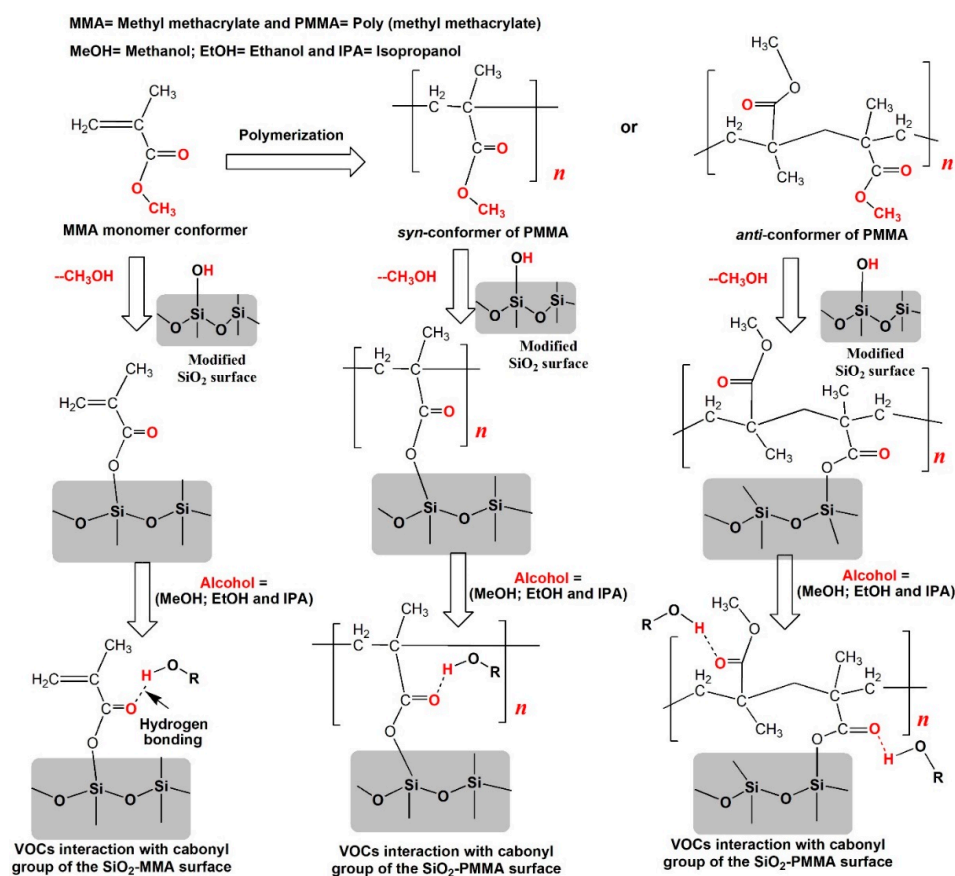


**Figure 2.** Proposed hypothetical steps for the coating of PMMA onto the MCL surfaces and the binding mode (via hydrogen bonding) of the VOCs with the PMMA.

### 3. Results

#### 3.1. MCL Deflection Measurements

All experiments were conducted using PMMA as the VOC sensing layers on the MCL surfaces only with the carrier gas without, and in the presence of methanol, ethanol, and isopropanol vapors at each of the three different concentrations. As controls, the MCL was tested both with and without the sensing PMMA layers, in the absence of the alcohol vapors, Figure 3 shows the deflection of the MCL alone, as a function of time at different concentrations of the VOC analytes and in the static mode [25]. The appearance of a clear baseline (shown as the green plot) devoid of vibration indicates that the sensor was unaffected by the carrier gas flow, external vibration, or thermal effects. Substantial deflections were observed with methanol and ethanol vapors for all three concentrations. However, for all three concentrations of isopropanol vapor, only weak deflections were observed. Clearly, the more volatile, smaller, and polar methanol molecules saturated the PMMA-coated MCL surfaces faster than the other two alcohols.

The calculations for these determinations are shown in Table 1. The validity of the methodology was ascertained by conducting experiments with methanol in which different volumes (i.e., 4.0, 6.0, and 8.0 mL) were used as the reservoir in separate experiments at 23 °C. The MCL deflection results showed only a small 4–5% standard deviation. As can be seen in Figure 3, the baselines initially reveal a negative deflection due to the change in pressure as the flow of the dry nitrogen carrier gas enters the sensing chamber and the ensuing moisture removal from the PMMA surface, which has been shown to be relatively insensitive towards water vapor exposure [25]. Within a few seconds, the target VOC molecules reach the cantilever chamber, and their interaction with the MCL coated with the PMMA sensing layer molecules results in the observed deflections, which appeared after approximately only 13 s. Table 1 shows the data for the deflections for each of the alcohol

vapors and their concentrations recorded at up to 580 s. Over the same time ranges, the MCL deflections as a function of the different concentrations were linear, as can be seen in Figure 4.

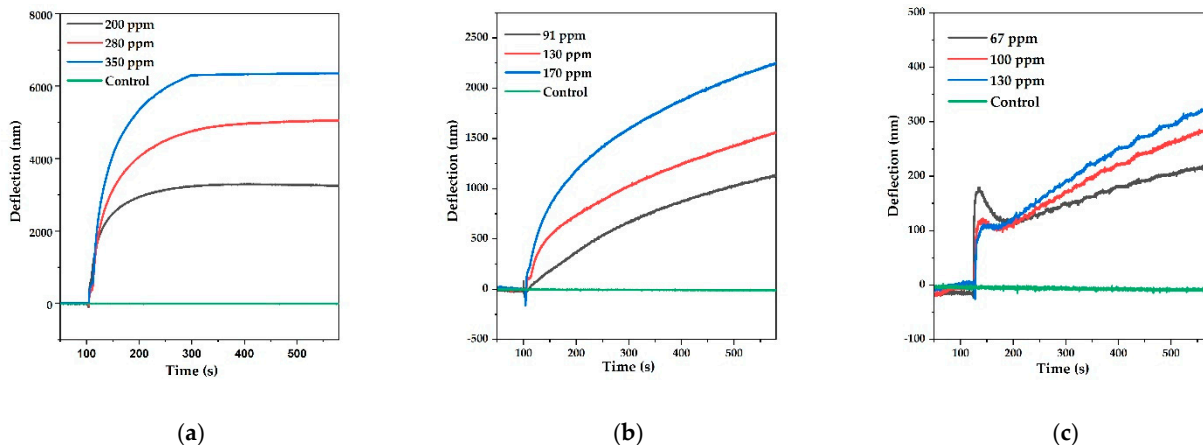


**Figure 3.** Microcantilever deflection versus time profiles for the different concentrations of (a) methanol, (b) ethanol, and (c) isopropanol vapors.

**Table 1.** Microcantilever deflection values at 580s for the alcohol vapor analytes at the different vapor pressures and corresponding concentrations measured.

Analyte	Vapor Pressure (Vp) (kPa)	mg	Concentration (mg/L = ppm)	Deflection (nm)
Methanol	15.2	4.95	200	$3.3 \times 10^3 \pm (4.59\%)$
	21.8	6.93	280	$4.8 \times 10^3 \pm (5.16\%)$
	27.9	8.72	350	$6.4 \times 10^3 \pm (5.81\%)$
Ethanol	6.97	2.26	91	$1.1 \times 10^3 \pm (5.24\%)$
	10.4	3.30	130	$1.7 \times 10^3 \pm (6.41\%)$
	13.7	4.28	170	$2.2 \times 10^3 \pm (6.18\%)$
Isopropanol	5.14	1.67	67	$1.9 \times 10^2 \pm (4.87\%)$
	7.88	2.50	100	$2.9 \times 10^2 \pm (6.28\%)$
	10.5	3.29	130	$3.9 \times 10^2 \pm (5.06\%)$

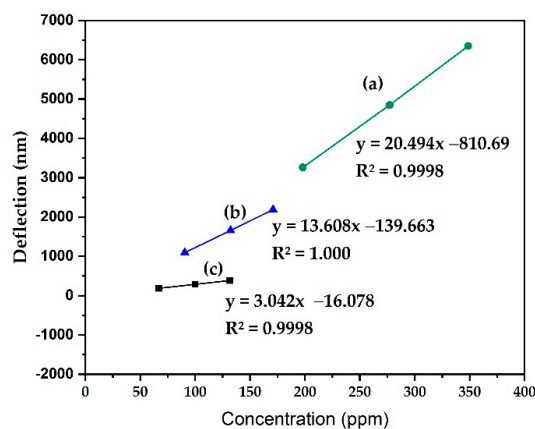


**Figure 4.** Concentration vs. deflection plots of the PMMA-coated MCLs to the (a) methanol (MeOH); (b) ethanol (EtOH) and (c) isopropanol (IPA) vapor.

Figure 5 compares the sensitivity of the PMMA-coated MCL towards the three different alcohol vapors as a function of the deflections (nm) vs. vapor concentrations (in ppm). These values compare favorably with those reported by Steffans et al. [28] and others [25–27] for methanol and ethanol vapors measured with their systems.

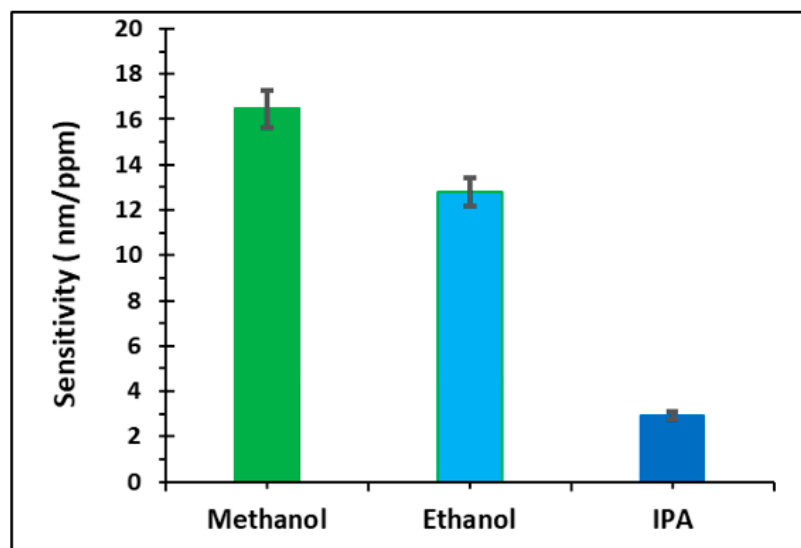


**Figure 5.** Sensitivity  $\pm$  ~5% of the PMMA-coated MCLs to the three alcohol vapors tested.

### 3.2. Quantum Chemical DFT Calculations

The DFT and other quantum chemical calculations were conducted to investigate the electrostatic interactions between the PMMA with alcohol vapors tested. We hypothesized that the alcohol vapor analytes are adsorbed onto the MCL surface PMMA layer by electrostatic hydrogen bonding interactions between the alcohol hydroxyl groups and the carbonyl groups of the PMMA, as is depicted in Figure 2. Our experimental data supports our hypothesis since control experiments using uncoated MCLs showed that there were no deflections and only stable baselines (Figure 3) could be recorded, thus indicating no interactions of the vapor molecules with the uncoated MCL silica surfaces.

To simplify the quantum chemical calculations and reduce the computation time, the DFT calculations were conducted using a monomeric and modeled tetrameric (“TMMA”) partial segments of the PMMA as isotactic *all-syn* “sTMMA” (Figure 6) and as syndiotactic *all-anti* “aTMMA” (Figure 7) segments of PMMA bound to the corresponding SiO<sub>2</sub>. The figures depict the idealized minimized conformations in which adjacent monomeric units are either *syn* (or isotactic) or *anti* (syndiotactic) to each other and are covalently attached to the corresponding SiO<sub>2</sub> surface segments of the MCLs. The optimized molecular structures of MMA and the PMMA tetramers and their binding modes with 1 to 4 molecules of either methanol, ethanol, or isopropanol are also shown in Figures 6 and 7. Table 2 shows the comparison of the resulting electronic binding interaction energies ( $\Delta$ IE kJ/mole) with both uncorrected and corrected BSSE values. Negative  $\Delta$ IE values correlate with favorable interactions.

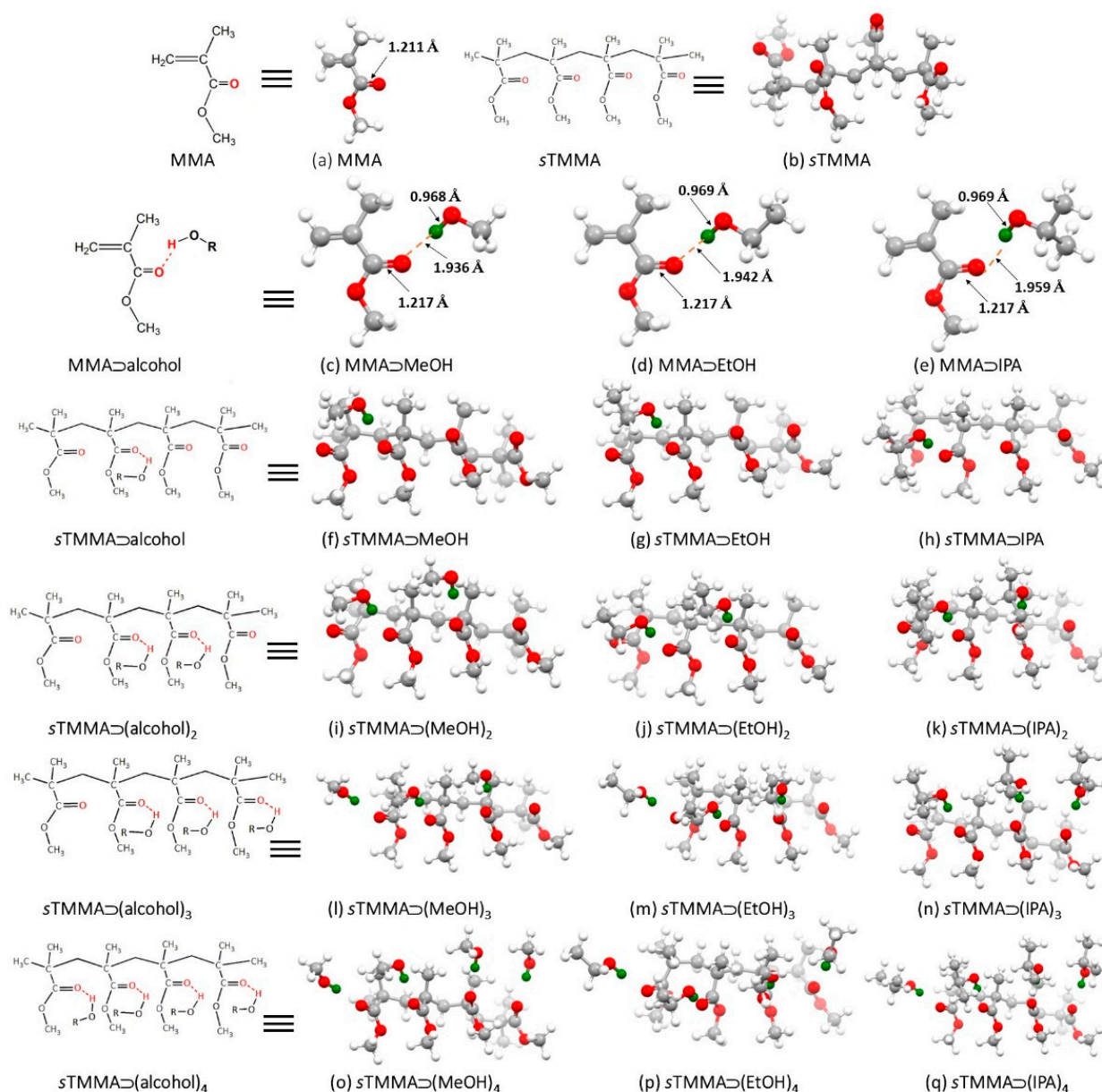


**Figure 6.** Formulas and optimized ball-and-stick molecular structures of: Top row: (a) MMA, (b) the *all-syn*-tetrameric segment of PMMA (“sTMMA”). Second row: (c) MMA ⊃ MeOH, (d) MMA ⊃ EtOH and (e) MMA ⊃ IPA. Third row: (f) sTMMA ⊃ MeOH, (g) sTMMA ⊃ EtOH and (h) sTMMA ⊃ IPA. Fourth row: (i) sTMMA ⊃ (MeOH)<sub>2</sub>, (j) sTMMA ⊃ (EtOH)<sub>2</sub> and (k) sTMMA ⊃ (IPA)<sub>2</sub>. Fifth row: (l) sTMMA ⊃ (MeOH)<sub>3</sub>, (m) sTMMA ⊃ (EtOH)<sub>3</sub> and (n) sTMMA ⊃ (IPA)<sub>3</sub>. Sixth row: (o) sTMMA ⊃ (MeOH)<sub>4</sub>, (p) sTMMA ⊃ (EtOH)<sub>4</sub> and (q) sTMMA ⊃ (IPA)<sub>4</sub>. Color code: carbon = black grey, oxygen atom = red, and all hydrogen atoms = white except for the alcohol hydrogen atoms = green.



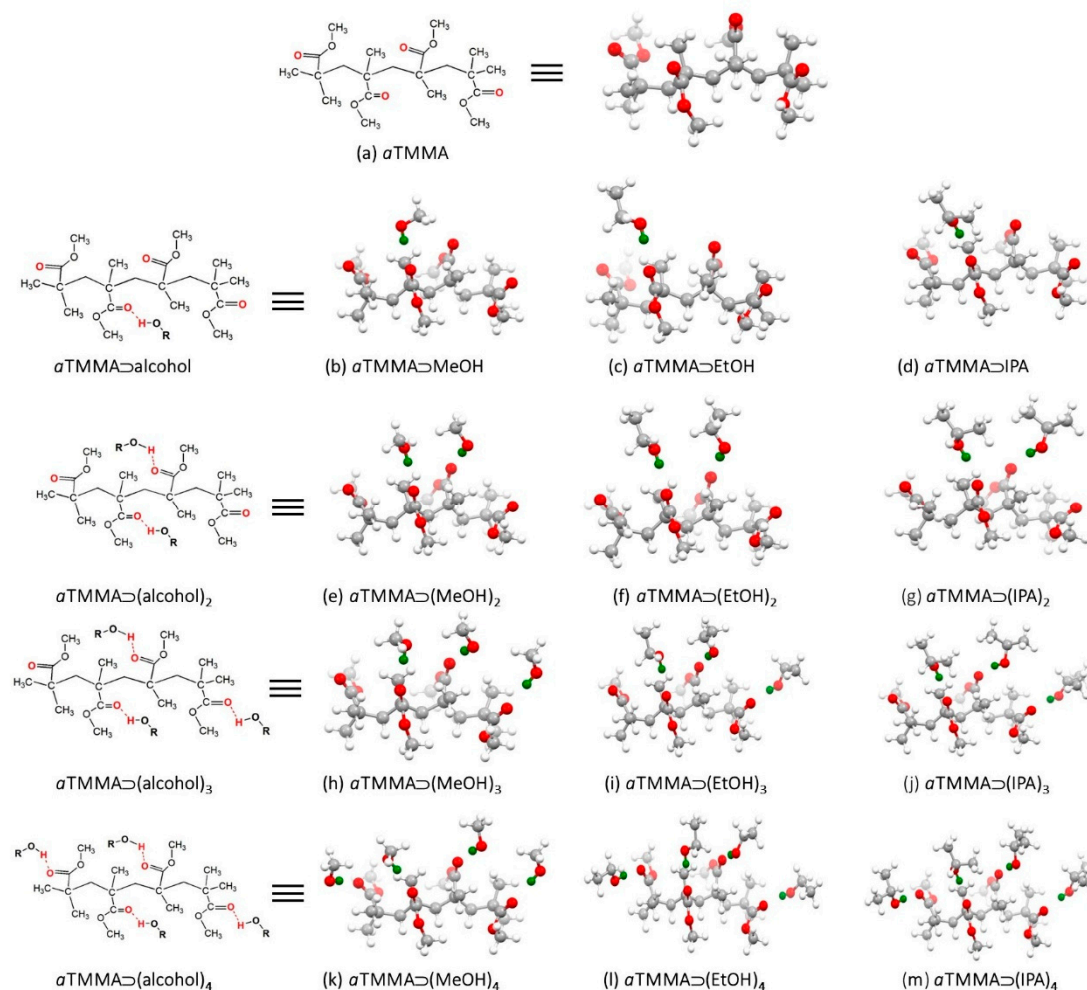


**Figure 7.** Formulas and optimized ball-and-stick molecular structures of *all-anti*-tetrameric segment of PMMA (“*a*TMMA”) with MeOH, EtOH, and IPA. Top row: (a) Free *a*TMMA. Second row: (b) *a*TMMA ⊃ MeOH, (c) *a*TMMA ⊃ EtOH and (d) *a*TMMA ⊃ PA. Third row: (e) *a*TMMA ⊃ (MeOH)<sub>2</sub>, (f) *a*TMMA ⊃ (EtOH)<sub>2</sub> and (g) *a*TMMA ⊃ (IPA)<sub>2</sub>. Fourth row: (h) *a*TMMA ⊃ (MeOH)<sub>3</sub>, (i) *a*TMMA ⊃ (EtOH)<sub>3</sub> and (j) *a*TMMA ⊃ (IPA)<sub>3</sub>. Fifth row: (k) *a*TMMA ⊃ (MeOH)<sub>4</sub>; (l) *a*TMMA ⊃ (EtOH)<sub>4</sub>; (m) *a*TMMA ⊃ (IPA)<sub>4</sub>. Color code: carbon = black grey, oxygen atom = red, and all hydrogen atoms = white except for the alcohol hydrogen atoms = green.

**Table 2.** Comparison of DFT-calculated electronic binding interaction energies ( $\Delta$ IE kJ/mole) for the alcohol vapor complexes of MMA; *s*TMMA and *a*TMMA with 1 to 4 equivalents of the corresponding alcohols (methanol, ethanol, and isopropanol) at the B3LYP/6-311++G(d,p) the gas phase level of theory.

Complex	Electronic Interaction Energies ( $\Delta$ IE kJ/mole) of the VOC Analytes					
	Methanol		Ethanol		Isopropanol	
	Uncorrected BSSE	Corrected BSSE	Uncorrected BSSE	Corrected BSSE	Uncorrected BSSE	Corrected BSSE
[MMA] ⊃ [analyte] (1:1)	−22.38	−20.62	−21.58	−19.92	−20.74	−19.07
[ <i>s</i> TMMA] ⊃ [analyte] (1:1)	−22.35	−19.03	−21.02	−18.10	−20.07	−17.23
[ <i>a</i> TMMA] ⊃ [analyte] (1:1)	−18.09	−16.05	−18.02	−15.45	−16.99	−14.78
[ <i>s</i> TMMA] ⊃ [analyte] (1:2)	−42.82	−36.80	−40.58	−34.97	−38.68	−33.29

Table 2. Cont.

Complex	Electronic Interaction Energies ( $\Delta E$ kJ/mole) of the VOC Analytes					
	Methanol		Ethanol		Isopropanol	
	Uncorrected BSSE	Corrected BSSE	Uncorrected BSSE	Corrected BSSE	Uncorrected BSSE	Corrected BSSE
[ <i>a</i> TMMA] $\supset$ [analyte] (1:2)	−39.99	−35.23	−37.66	−33.15	−34.52	−30.31
[ <i>s</i> TMMA] $\supset$ [analyte] (1:3)	−64.59	−56.82	−61.47	−54.24	−58.99	−51.74
[ <i>a</i> TMMA] $\supset$ [analyte] (1:3)	−62.91	−56.96	−59.17	−52.71	−56.19	−49.66
[ <i>s</i> TMMA] $\supset$ [analyte] (1:4)	−86.63	−76.31	−82.50	−72.81	−79.10	−69.43
[ <i>a</i> TMMA] $\supset$ [analyte] (1:4)	−84.34	−76.28	−80.47	−71.76	−77.82	−69.12

#### 4. Conclusions

PMMA has had many applications which have been extensively reviewed [36–39]. In the present study, we have shown that PMMA was a suitable and stable polymer coating for the silica surfaces of MCLs and was capable of being used to detect volatile alcohol vapors. Our findings were in agreement with the findings from two earlier reports [25,26]. Shin et al. [27] reported the detection of methanol and ethanol vapors on PMMA-coated piezoelectric microcantilevers with sensitivities of 0.03 Hz/ppm and 0.01 Hz/ppm, respectively. The MCL response times reported herein were much faster than those reported by Shin et al. and also by Steffens et al. [28], who used a polyaniline coated sensing layer. The modes of exposure to the same two volatile liquids reported by these latter two groups were also different from ours.

The magnitude of the MCL deflections showed linear deflection vs. concentration responses. That stable baselines over the time periods examined suggests that the PMMA layer could be covalently bound to the SiO<sub>2</sub> surfaces and supports the hypothesis proposed for the DFT study. Methanol, the most volatile of the three alcohol vapors tested, showed the highest responses compared to those of ethanol and isopropanol vapor molecules. The generation of the target molecule vapors inside a custom-made vapor generating chamber was a convenient way to generate different concentrations of the vapors of volatile organic liquids and resulted in rapid, reproducible, and quantifiable microcantilever deflections. These findings could be extended in a more general sense towards the MCL sensor device being used for highly sensitive and rapid detection(s) of these and potentially other VOC vapors in the air.

Finally, the DFT-calculated electrostatic electronic interaction energies in all cases were consistent with the experimental results and were in general support for the hypothetical basis for the modes of interaction between the analyte alcohols and the PMMA sensing layer on the silica MCL surfaces. The molecular electrostatic surface potentials [40,41] of MMA and PMMA and their complexes with alcohols (methanol, ethanol, and isopropanol) are shown in Figures 8–10. The surfaces were formed by mapping the electrostatic potentials (MESPs) onto their HOMO electron density surfaces. The ESPs show the relative polarities and thus the reactive sites of the species: the negative ESP are shown in red, and the order of increasing electrostatic potentials (i.e., highest–ve value) is: red > orange > yellow > green > blue. From Figures 8–10, it was clearly evident that the carbonyl oxygen (C=O) atom of the ligands (MMA and PMMA) contain high electron density, as shown in red color (Figure 8, ESP) and are the most preferable sites for electrophilic attack and interaction with the nucleophilic partially positive charged hydroxyl hydrogen atoms (blue color) of the alcohols (methanol, ethanol, and isopropanol). As can be seen, the negative potentials are generated over the more electronegative oxygen atom, whereas the H-atom exhibits a positive potential region in the structures (represented by the blue color located around the hydrogen atom of the alcohol hydroxyl group). The yellow color indicates the slightly rich electron regions, and the green reflects more neutral zones.

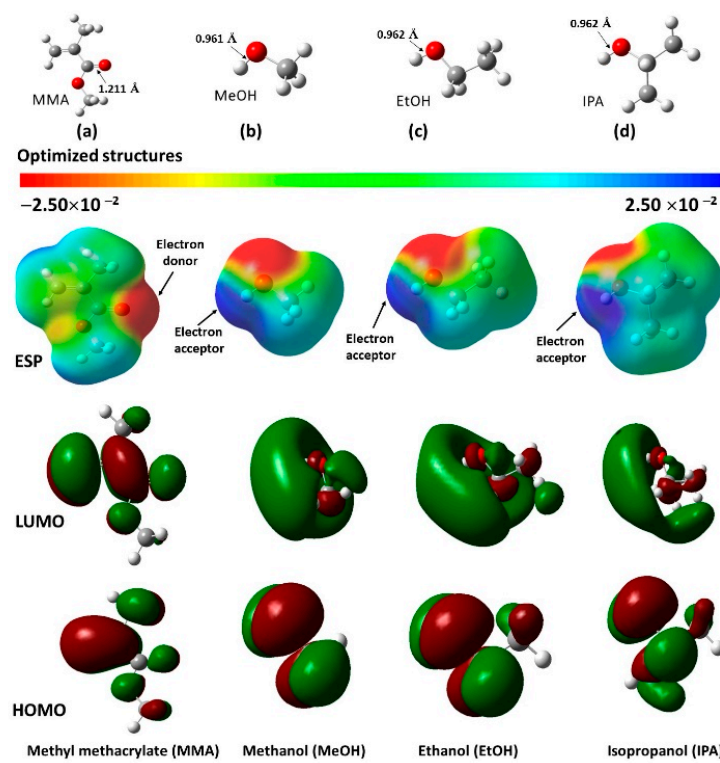


**Figure 8.** Optimized gas phase molecular structures, ESPs, LUMOs, and HOMOs structures of (a) MMA, (b) methanol (MeOH); (c) ethanol (EtOH), and (d) isopropanol (IPA) at the B3LYP/6-311++G(d,p) level of theory.

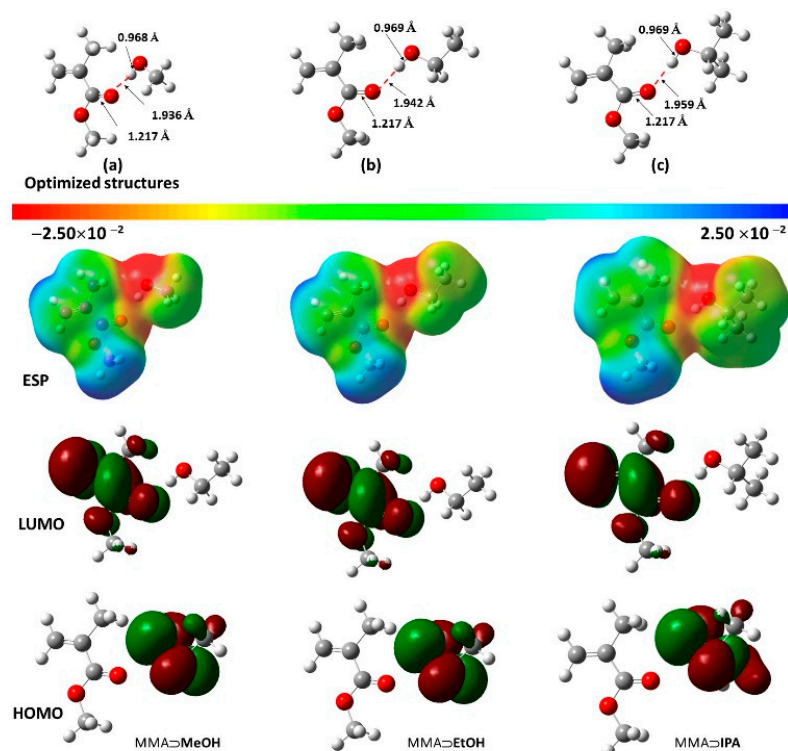


**Figure 9.** Optimized gas phase molecular structures, ESP, LUMOs, and HOMOs structures of MMA 1:1 complexes with alcohols: (a) MMA ⊃ MeOH; (b) MMA ⊃ EtOH; and (c) MMA ⊃ IPA at the B3LYP/6-311++G(d,p) level of theory.

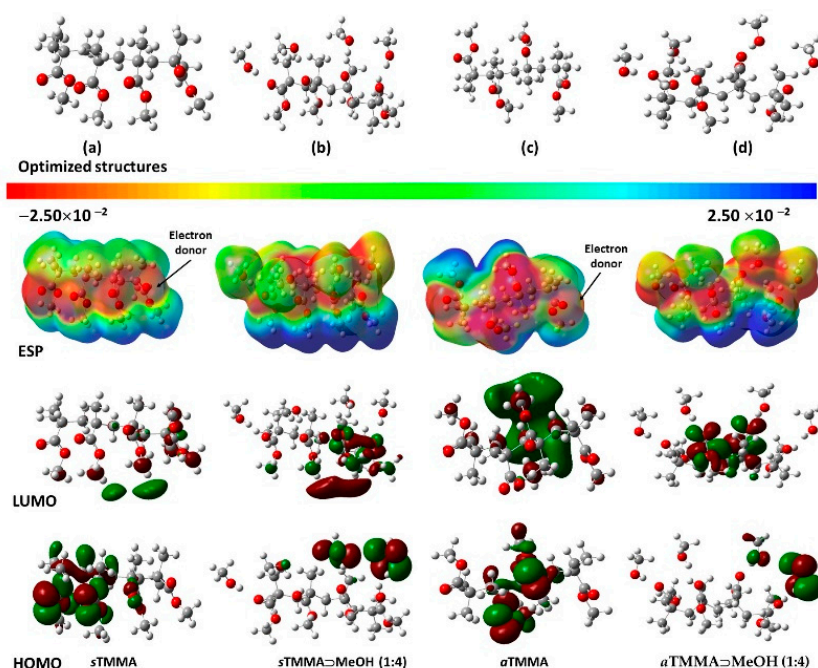


**Figure 10.** Optimized gas phase molecular structures, ESP, LUMOs and HOMOs structures of *s*TMMA; *a*TMMA and their 1:4 complexes with methanol: (a) *s*TMMA; (b) *s*TMMA  $\supset$  MeOH; (c) *a*TMMA; and (d) *a*TMMA  $\supset$  MeOH at the B3LYP/6-311++G(d,p) level of theory.

The ESP data presented in Table 3 indicate the following:

- The reactivity of the MMA was clearly greater than that of the two tetrameric segments (i.e., *s*TMMA and *a*TMMA). This was reflected in the larger electronegativity ( $\chi$ ) and electrophilicity Index ( $\omega$ ) of MMA. This is to be expected since MMA is easily polymerized.
- The data for the 1:1 MMA:alcohol complexes show very few differences in their values.
- The difference in stability between the two tetrameric segments (*s*TMMA and *a*TMMA) as measured using their HOMO-LUMO gaps ( $\Delta E_{\text{gap}}$ ) was relatively small (0.130 eV), whereas there was a much larger relative difference between the EAs (0.268 eV), the  $\omega$  values (0.284 eV) and the dipole moments (3.774 Debyes), shown for the *a*TMMA over the *s*TMMA. The higher dipole moment for the *a*TMMA could be easily visualized from the ESP map shown in Figure 10c. This could account for the stronger binding of the isotactic polymer (used in this study) to the silicon surface.
- In contrast, the stability for the model 1:4 complexes of *s*TMMA vs. *a*TMMA binding with methanol (and the other alcohols) favors the *s*TMMA.

**Table 3.** HOMO-LUMO gap ( $\Delta E_{\text{gap}}$ ), ionization potential (IP), electron affinity (EA), electronegativity ( $\chi$ ), chemical potential ( $\mu$ ), hardness ( $\eta$ ), softness (*S*), electrophilicity index ( $\omega$ ) and dipole moments (dm) of MMA; *s*TMMA; *a*TMMA and their complexes with alcohols (methanol; ethanol and isopropanol) at the B3LYP/6-311++G(d,p) level of theory. (gas phase).

	$E_{\text{HOMO}}$ (eV)	$E_{\text{LUMO}}$ (eV)	$\Delta E_{\text{gap}}$ (eV)	IP (eV)	EA (eV)	$\chi$ (eV)	$\mu$ (eV)	$\eta$ (eV)	<i>S</i> (eV)	$\omega$ (eV)	dm (Debye)
[MMA]	−7.605	−1.525	−6.080	7.605	1.525	4.565	−4.565	3.040	0.329	3.427	1.763
[ <i>s</i> TMMA]	−7.467	−0.477	−6.990	7.467	0.477	3.972	−3.972	3.495	0.286	2.257	6.031
[ <i>a</i> TMMA])	−7.605	−0.745	−6.860	7.605	0.745	4.175	−4.175	3.430	0.292	2.541	9.805
[MeOH]	−7.737	−0.360	−7.377	7.737	0.360	4.048	−4.048	3.689	0.271	2.222	1.890

Table 3. Cont.

	$E_{HOMO}$ (eV)	$E_{LUMO}$ (eV)	$\Delta E_{gap}$ (eV)	$IP$ (eV)	$EA$ (eV)	$\chi$ (eV)	$\mu$ (eV)	$\eta$ (eV)	$S$ (eV)	$\omega$ (eV)	$dm$ (Debye)
[EtOH]	−7.636	−1.525	−6.111	7.636	1.525	4.580	−4.580	3.055	0.327	3.433	1.761
[IPA]	−7.597	−1.795	−5.803	7.597	1.795	4.696	−4.696	2.901	0.345	3.800	1.770
[MMA] ⊃ [MeOH] (1:1)	−6.990	−1.795	−5.195	6.990	1.795	4.392	−4.392	2.597	0.385	3.713	3.429
[MMA] ⊃ [EtOH] (1:1)	−6.938	−1.785	−5.152	6.938	1.785	4.362	−4.362	2.576	0.388	3.692	3.368
[MMA] ⊃ [IPA] (1:1)	−6.961	−1.773	−5.188	6.961	1.773	4.367	−4.367	2.594	0.386	3.677	3.289
[sTMMA] ⊃ [MeOH] (1:4)	−6.850	−0.690	−6.160	6.850	0.690	3.770	−3.770	3.080	0.325	2.308	10.361
[aTMMA] ⊃ [MeOH] (1:4)	−6.709	−0.991	−5.718	6.709	0.991	3.850	−3.850	2.859	0.350	2.592	9.373
[sTMMA] ⊃ [EtOH] (1:4)	−6.777	−0.680	−6.097	6.777	0.680	3.729	−3.729	3.048	0.328	2.280	9.410
[aTMMA] ⊃ [EtOH] (1:4)	−6.846	−0.898	−5.948	6.846	0.898	3.872	−3.872	2.974	0.336	2.520	8.960
[sTMMA] ⊃ [IPA] (1:4)	−6.778	−0.682	−6.095	6.778	0.682	3.730	−3.730	3.048	0.328	2.283	6.372
[aTMMA] ⊃ [IPA] (1:4)	−6.609	−1.046	−5.562	6.609	1.046	3.827	−3.827	2.781	0.360	2.634	11.586

Future investigations will use a vapor-generated approach combined with a microcantilever device to detect other VOCs.

**Supplementary Materials:** The input and output files for the DFT calculation for all the geometry optimized structures reported can be downloaded at: <https://www.mdpi.com/article/10.3390/chemosensors10110452/s1>.

**Author Contributions:** Conceptualization, A.N.A., M.A.A.-G., R.A.A. and S.R.; methodology, H.A., A.K.A. and K.E.A.; validation, A.N.A., M.A.A.-G. and S.R.; investigation, R.S., F.A., F.S.A. and A.F.A.; data analysis, F.S.A., F.A., R.S., H.A., A.K.A., K.E.A. and A.F.A.; writing—original draft preparation, A.N.A., M.A.A.-G., S.R. and R.A.A.; writing—review and editing, A.N.A., M.A.A.-G., S.R. and P.E.G.; supervision, A.N.A., R.A.A., A.K.A., K.E.A., S.R. and P.E.G.; software, S.R.; funding acquisition, A.N.A. and H.A. All authors have read and agreed to the published version of the manuscript.

**Funding:** The authors extend their appreciation to the Deputyship for Research & Innovation, Ministry of Education in Saudi Arabia for funding this research work through the project no. (IFKSURG-2-63).

**Institutional Review Board Statement:** Not applicable.

**Informed Consent Statement:** Not applicable.

**Data Availability Statement:** Any additional data in support of the findings of this study besides those provided as Supplementary Materials are available from the corresponding author upon reasonable request.

**Acknowledgments:** The DFT and quantum chemical computations were enabled by the support in part provided by Oliver Stueker at Acenet and the Digital Research Alliance of Canada who are gratefully appreciated.

**Conflicts of Interest:** The authors declare no conflict of interest.

## References

- David, E.; Niculescu, V.C. Volatile organic compounds (VOCs) as environmental pollutants: Occurrence and mitigation using nanomaterials. *Int. J. Environ. Res. Public Health* **2021**, *18*, 13147. [[CrossRef](#)] [[PubMed](#)]
- Li, Y.; Yan, B. Human health risk assessment and distribution of VOCs in a chemical site, Weinan, China. *Open Chem.* **2022**, *20*, 192–203. [[CrossRef](#)]
- Taylor, S.M.; Sider, D.; Hampson, C.; Taylor, S.J.; Wilson, K.; Walter, S.D.; Eyles, J.D. Community health effects of a petroleum refinery. *Ecosyst. Health* **2008**, *3*, 27–43. [[CrossRef](#)]
- Fung, A.G.; Rajapakse, M.Y.; McCartney, M.M.; Falcon, A.K.; Fabia, F.M.; Kenyon, N.J.; Davis, C.E. Wearable environmental monitor to quantify personal ambient volatile organic compound exposures. *ACS Sens.* **2019**, *4*, 1358–1364. [[CrossRef](#)] [[PubMed](#)]
- Seifert, B.; van de Wiel, H.J.; Dodet, B.; O'Neill, I.K. (Eds.) *Volatile Organic Compounds in Environmental Carcinogens. Methods of Analysis and Exposure Measurement. Volume 12—Indoor Air*; International Agency for Research on Cancer: Lyon, France, 1993; Volume 109, pp. 245–250, ISBN-13: 978-9283221098.

6. World Health Organization. *WHO Guidelines for Indoor Air Quality: Selected Pollutants*; World Health Organization, Regional Office for Europe: Copenhagen, Denmark, 2010. Available online: <https://apps.who.int/iris/handle/10665/260127> (accessed on 21 August 2022).
7. Volatile Organic Compounds. Available online: <https://www.lung.org/clean-air/at-home/indoor-air-pollutants/volatile-organic-compounds>. (accessed on 28 July 2022).
8. Haick, H.; Broza, Y.; Mochalski, P.; Ruzsanyi, V.; Amann, A. Assessment, origin, and implementation of breath volatile cancer markers. *Chem. Soc. Rev.* **2014**, *43*, 1423–1449. [[CrossRef](#)]
9. Török, Z.-M.; Blaser, A.F.; Kavianiyejad, K.; de Torrella, C.G.M.G.; Nsubuga, L.; Mishra, Y.K.; Rubahn, H.-G.; de Oliveira Hansen, R. Breath Biomarkers as Disease Indicators: Sensing Techniques. Approach for Detecting Breath Gas and COVID-19. *Chemosensors* **2022**, *10*, 167. [[CrossRef](#)]
10. Kraut, J.A.; Mullins, M.E. Toxic Alcohols. *N. Engl. J. Med.* **2018**, *378*, 270–280. [[CrossRef](#)]
11. Birková, A.; Hubková, B.; Čižmárová, B.; Bolerázka, B. Current view on the mechanisms of alcohol-mediated toxicity. *Int. J. Mol. Sci.* **2021**, *22*, 9686. [[CrossRef](#)]
12. Rezende, G.C.; Le Calvé, S.; Brandner, J.J.; Newport, D. Micro photoionization detectors. *Sens. Actuators B Chem.* **2019**, *287*, 86–94. [[CrossRef](#)]
13. Shiokawa, S.; Kondoh, J. Surface acoustic wave sensors. *Jpn. J. Appl. Phys.* **2004**, *43*, 2799. [[CrossRef](#)]
14. Constantinou, I.; Viespe, C. Detection of volatile organic compounds using surface acoustic wave sensor based on nanoparticles incorporated in polymer. *Coatings* **2019**, *9*, 373. [[CrossRef](#)]
15. Bur, C.; Andersson, M.E.; Spetz, A.L.; Schütze, A. Detecting volatile organic compounds in the ppb range with gas sensitive platinum gate SiC-field effect transistors. *IEEE Sens. J.* **2014**, *14*, 3221–3228. [[CrossRef](#)]
16. Lerchner, J.; Caspary, D.; Wolf, G. Calorimetric detection of volatile organic compounds. *Sens. Actuators B Chem.* **2000**, *70*, 57–66. [[CrossRef](#)]
17. Lourenço, C.; Bergin, S.; Hodgkinson, J.; Francis, D.; Staines, S.E.; Saffell, J.R.; Walton, C.; Tatam, R.P. Instrumentation for quantitative analysis of volatile compounds emission at elevated temperatures. Part 1: Design and implementation. *Sci. Rep.* **2020**, *10*, 8700. [[CrossRef](#)]
18. Georghiou, P.E.; Snow, D.; Williams, D.T. Formaldehyde monitoring in urea-formaldehyde foam-insulated houses in St. John's, Newfoundland, Canada: Correlative field evaluation of a real-time infrared spectrophotometric method. *Environ. Int.* **1983**, *9*, 279–287. [[CrossRef](#)]
19. Thundat, T.; Chen, G.Y.; Warmack, R.J.; Allison, D.P.; Wachter, E.A. Vapor detection using resonating microcantilevers. *Anal. Chem.* **1995**, *67*, 519–521. [[CrossRef](#)]
20. Maute, M.; Raible, S.; Prins, F.E.; Kern, D.P.; Ulmer, H.; Weimar, U.; Göpel, W. Detection of volatile organic compounds (VOCs) with polymer-coated cantilevers. *Sens. Actuators B Chem.* **1999**, *58*, 505–511. [[CrossRef](#)]
21. Fadel, L.; Lochon, F.; Dufour, I.; Français, O. Chemical sensing: Millimeter size resonant microcantilever performance. *J. Microeng. Microeng.* **2004**, *14*, S23. [[CrossRef](#)]
22. Dong, Y.; Gao, W.; You, Z. Trace gas sensor based on MEMS cantilever resonator. *Adv. Mat. Res.* **2011**, *383–390*, 3115–3120. [[CrossRef](#)]
23. Mamou, D.; Nsubuga, L.; Lisboa Marcondes, T.; Høegh, S.O.; Hvam, J.; Niekkel, F.; Lofink, F.; Rubahn, H.-G.; de Oliveira Hansen, R. Surface modification enabling reproducible cantilever functionalization for industrial gas sensors. *Sensors* **2021**, *21*, 6041. [[CrossRef](#)]
24. Risplendi, F.; Ricci, A.; Cicero, G. Functionalization layer effect on the mechanical properties of silicon based micro-cantilever mass sensors: A theoretical study. *Sens. Actuators B Chem.* **2014**, *195*, 177–180. [[CrossRef](#)]
25. Battiston, F.M.; Ramseyer, J.-P.; Lang, H.P.; Baller, M.K.; Gerber, C.; Gimzewski, J.K.; Meyer, E.; Güntherodt, H.-J. A chemical sensor based on a microfabricated cantilever array with simultaneous resonance-frequency and bending readout. *Sens. Actuators B Chem.* **2001**, *77*, 122–131. [[CrossRef](#)]
26. Misiakos, K.; Raptis, I.; Goustouridis, D.; Kitsara, M.; Contopanagos, H.; Gerardino, A.; Valamontes, E. Ultra-miniaturized monolithically integrated polymer coated Si optoelectronic cantilevers for gas sensing applications. In Proceedings of the SENSORS, 2009 IEEE, Christchurch, New Zealand, 25–28 October 2009; pp. 429–432. [[CrossRef](#)]
27. Shin, S.; Paik, J.K.; Lee, N.E.; Park, J.S.; Park, H.D.; Lee, J. Gas sensor application of piezoelectric cantilever nanobalance; electrical signal read-out. *Ferroelectrics* **2005**, *328*, 59–65. [[CrossRef](#)]
28. Steffens, C.; Leite, F.L.; Manzoli, A.; Sandoval, R.D.; Fatibello, O.; Herrmann, P.S.P. Microcantilever sensors coated with a sensitive polyaniline layer for detecting volatile organic compounds. *J. Nanosci. Nanotechnol.* **2014**, *14*, 6718–6722. [[CrossRef](#)]
29. Al-Gawati, M.A.; Alhazaa, A.; Albrithen, H.; Alnofiay, J.; Alodhayb, A. Effect of surface patterning using femtosecond laser on micromechanical and structural properties of micromechanical sensors. *Mater. Res. Express* **2020**, *7*, 085904. [[CrossRef](#)]
30. Aloraini, D.A.; Almuqrin, A.H.; Alanazi, A.; Ain, Q.T.; Alodhayb, A.N. Rapid and sensitive detection of severe acute respiratory syndrome coronavirus 2 in label-free manner using micromechanical sensors. *Sensors* **2021**, *21*, 4439. [[CrossRef](#)] [[PubMed](#)]
31. Frisch, M.J.; Trucks, G.W.; Schlegel, H.B.; Scuseria, G.E.; Robb, M.A.; Cheeseman, J.R.; Scalmani, G.; Barone, V.; Petersson, G.A.; Nakatsuji, H.; et al. *Gaussian 16, Revision C.01*; Gaussian, Inc.: Wallingford, CT, USA, 2019.
32. Kestner, N.R.; Combariza, J.E. *Basis Set Superposition Errors: Theory and Practice. Reviews in Computational Chemistry*; Wiley-VCH, John Wiley and Sons, Inc.: New York, NY, USA, 1999; Volume 13, p. 99. [[CrossRef](#)]

33. Fukui, K.; Yonezawa, T.; Shingu, H. A molecular orbital theory of reactivity in aromatic hydrocarbons. *J. Chem. Phys.* **1952**, *20*, 722–725. [[CrossRef](#)]
34. Koopmans, T. Ordering of wave functions and eigenvalues to the individual electrons of an atom. *Physica* **1933**, *1*, 104–113. [[CrossRef](#)]
35. Luo, J.; Xue, Z.Q.; Liu, W.M.; Wu, J.L.; Yang, Z.Q. Koopmans' theorem for large molecular systems within density functional theory. *J. Phys. Chem. A* **2006**, *110*, 12005–12009. [[CrossRef](#)]
36. Ali, U.; Karim, K.J.B.; Buang, N.A. A Review of the properties and applications of poly (methyl methacrylate) (PMMA). *Polym. Rev.* **2015**, *55*, 678–705. [[CrossRef](#)]
37. Henry, A.C.; Tutt, T.J.; Galloway, M.; Davidson, Y.Y.; McWhorter, C.S.; Soper, S.A.; McCarley, R.L. Surface modification of poly(methyl methacrylate) used in the fabrication of microanalytical devices. *Anal. Chem.* **2000**, *72*, 5331–5337. [[CrossRef](#)]
38. Shah, E.V.; Patel, C.M.; Roy, D.R. Structure, electronic, optical and thermodynamic behavior on the polymerization of PMMA: A DFT Investigation. *Comp. Biol. Chem.* **2018**, *72*, 192–198. [[CrossRef](#)] [[PubMed](#)]
39. Murray, J.S.; Politzer, P. The electrostatic potential: An overview. *Wiley Interdiscip. Rev. Comput. Mol. Sci.* **2011**, *1*, 153–163. [[CrossRef](#)]
40. Murray, J.S.; Sen, K. *Molecular Electrostatic Potentials, Concepts and Applications*; Elsevier: Amsterdam, The Netherlands, 1996. [[CrossRef](#)]
41. Politzer, P.; Murray, J. The fundamental nature and role of the electrostatic potential in atoms and molecules. *Theor. Chem. Acc.* **2002**, *108*, 134–142. [[CrossRef](#)]